

AD-A172 228

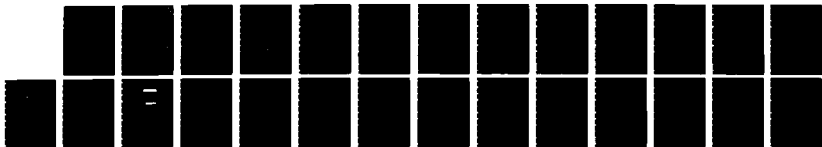
X-RAY SPECTROSCOPY WITH Z-PINCH NEON PLASMAS(U) NAVAL  
RESEARCH LAB WASHINGTON DC G MEHLMAN ET AL. 31 JUL 86  
NRL-MR-5833

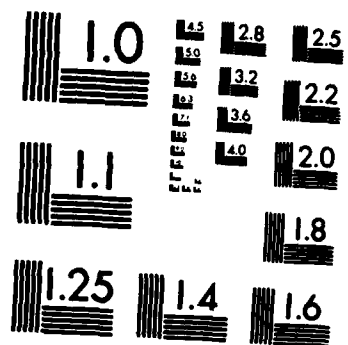
1/1

UNCLASSIFIED

F/G 20/9

NL





MICROCOPY RESOLUTION TEST CHART  
NATIONAL BUREAU OF STANDARDS-1963-A

AD-A172 228

# X-Ray Spectroscopy with Z-Pinch Neon Plasmas

G. MEHLMAN,\* P.G. BURKHALTER, D.A. NEWMAN,\* S.J. STEPHANAKIS,  
F.C. YOUNG, AND D.J. NAGEL

*Condensed Matter Physics Branch  
Condensed Matter and Radiation Sciences Division*

*\*Sachs/Freeman Associates, Inc.*

DTIC FILE COPY

DTIC  
ELECTE  
SEP 23 1986  
S  
B

Approved for public release; distribution unlimited.

86 9 23 087

SECURITY CLASSIFICATION OF THIS PAGE

AD-A172 225

REPORT DOCUMENTATION PAGE

1a REPORT SECURITY CLASSIFICATION UNCLASSIFIED		1b RESTRICTIVE MARKINGS	
2a SECURITY CLASSIFICATION AUTHORITY		3 DISTRIBUTION/AVAILABILITY OF REPORT Approved for public release; distribution unlimited.	
2b DECLASSIFICATION/DOWNGRADING SCHEDULE		4. PERFORMING ORGANIZATION REPORT NUMBER(S) NRL Memorandum Report 5833	
4. PERFORMING ORGANIZATION REPORT NUMBER(S) NRL Memorandum Report 5833		5. MONITORING ORGANIZATION REPORT NUMBER(S)	
6a NAME OF PERFORMING ORGANIZATION Naval Research Laboratory	6b OFFICE SYMBOL (if applicable) Code 4860	7a NAME OF MONITORING ORGANIZATION	
6c. ADDRESS (City, State, and ZIP Code) Washington, DC 20375-5000		7b. ADDRESS (City, State, and ZIP Code)	
8a. NAME OF FUNDING / SPONSORING ORGANIZATION Defense Nuclear Agency	8b. OFFICE SYMBOL (if applicable)	9. PROCUREMENT INSTRUMENT IDENTIFICATION NUMBER	
8c. ADDRESS (City, State, and ZIP Code) Washington, DC 20305-1000		10 SOURCE OF FUNDING NUMBERS	
		PROGRAM ELEMENT NO. 62715H	PROJECT NO. T99 QMLXA
		TASK NO.	WORK UNIT ACCESSION NO.
11 TITLE (include Security Classification) X-Ray Spectroscopy with Z-pinch Neon Plasmas			
12. PERSONAL AUTHOR(S) Mehlman,* G., Burkhalter, P.G., Newman,* D.A., Stephanakis, S.J., Young, F.C., and Nagel, D.J.			
13a. TYPE OF REPORT	13b TIME COVERED FROM TO	14. DATE OF REPORT (Year, Month, Day) 1986 July 31	15. PAGE COUNT 26
16. SUPPLEMENTARY NOTATION *Sachs/Freeman Associates, Inc.			
17 COSATI CODES		18 SUBJECT TERMS (Continue on reverse if necessary and identify by block number)	
FIELD	GROUP	SUB-GROUP	
19 ABSTRACT (Continue on reverse if necessary and identify by block number)			
<p style="text-align: right;">Nec.</p> <p>Spatially-resolved soft x-ray spectra were collected for neon plasmas produced by imploding hollow annular gas puffs with MA level driving currents. The Z-pinch imploded plasma were studied for different rise-time currents produced with or without the use of a plasma erosion opening switch (PEOS). Selected spectrograms were processed and analyzed to obtain absolute energies for the radiation emitted in the Ne IX and Ne X discrete transitions as well as for total emission over the spectral range 900-1600 eV. The energy radiated for typical shots with or without the PEOS is compared particularly for the predominant <math>\alpha</math> transitions of both ions. Also, line widths for the <math>\alpha</math> and <math>\beta</math> transitions of both ions are determined. <span style="float: right;">→ p 17</span></p>			
20 DISTRIBUTION/AVAILABILITY OF ABSTRACT <input type="checkbox"/> UNCLASSIFIED/UNLIMITED <input checked="" type="checkbox"/> SAME AS RPT <input type="checkbox"/> DTIC USERS		21 ABSTRACT SECURITY CLASSIFICATION UNCLASSIFIED	
22a NAME OF RESPONSIBLE INDIVIDUAL P.G. Burkhalter		22b TELEPHONE (Include Area Code) (202) 767-2154	22c OFFICE SYMBOL Code 4681

DD FORM 1473, 84 MAR

83 APR edition may be used until exhausted  
All other editions are obsolete

SECURITY CLASSIFICATION OF THIS PAGE

U.S. Government Printing Office: 1985-587-647

CONTENTS

INTRODUCTION..... 1  
EXPERIMENTAL ARRANGEMENT..... 2  
DATA ANALYSIS..... 5  
RESULTS..... 6  
SUMMARY..... 17  
APPENDIX..... 18  
REFERENCES..... 21

**S** DTIC ELECTE **D**  
SEP 23 1986  
B

Accession For	
NTIS GRANT	<input checked="" type="checkbox"/>
DDIC TAG	<input type="checkbox"/>
Unprocessed	<input type="checkbox"/>
Classification	
Availability Codes	
Dist	Special
A-1	



# X-RAY SPECTROSCOPY WITH Z-PINCH NEON PLASMA

## I. INTRODUCTION

The dense linear Z-pinch generated by imploding an annular gas column is a source of extreme UV and x-ray emission.<sup>1-6</sup> Highly ionized atoms, concentrated at high density along the Z axis by large electrical currents, emit intense lines from the excitation of L- and K-shell electrons.

Previous measurement<sup>7</sup> established that the energy delivered by the Gamble II generator at the Naval Research Laboratory to imploding plasma loads coupled efficiently to neon gas puffs so that neon plasmas provided the maximum yield of keV x-rays. The implosion of neon gas jets on the Gamble II generator has been described in terms of the current driving the implosion and the mass loading of the gas column. In addition, the incorporation of a plasma erosion opening switch (PEOS)<sup>8</sup> to sharpen the current risetime has produced Z-pinchs that appear more uniform axially and tighter radially.<sup>9</sup>

We have studied the K-shell emission spectra of neon plasmas produced by Gamble II implosions to assess the total x-ray yield in the keV region. In addition to producing a high yield of nearly monoenergetic x-ray radiation (~1 keV), these measurements are relevant to the two-component plasma (Na-Ne) with photopumping of neon by sodium for x-ray lasing.<sup>10,11</sup> Time-integrated spectra from 900 to 1600 eV were collected with a crystal spectrograph. The photographic spectra were digitized with a computerized densitometer, and the data, film density versus spectral distance, were reduced with a computer program<sup>12</sup> to obtain line intensities and line profiles. Thus, a major effort was devoted to the measurement of absolute line intensities in this x-ray energy range.

## II. EXPERIMENTAL ARRANGEMENT

### A. Plasma Source

The Gamble II generator delivers currents with peaks of up to 1.45 MA and with a risetime of approximately 60 nsec to implode an annular gas jet. Neon gas is puffed through a supersonic nozzle into a 4 cm anode-cathode gap to form an initial column with a mean radius of 1.25 cm and a gas thickness of  $\sim 0.3$  cm.<sup>13</sup> The neon gas is preionized with a UV flashboard source a few  $\mu$ s before the current pulse.

The neon K-shell radiation from these implosions was recorded with a crystal spectrograph, a filtered x-ray diode (XRD) and a filtered pinhole camera. All of these diagnostics viewed the imploded plasma at 90 degrees to the axis of the implosion. Total intensities deduced from these measurements are based on isotropic x-ray emission into  $4\pi$  sr.

X-ray spectra were recorded for implosions with a peak current of 1.2 MA. The current pulse and the corresponding XRD pulse for a shot without the PEOS are shown in Fig. 1a. The delay of the x-ray pulse indicates that the implosion occurs 135 ns after onset of the current. Comparisons of implosion-time and x-ray intensity measurements as a function of mass loading with a simple theoretical model simulating the implosion dynamics<sup>14</sup> indicates that the mass in the gas puff load is  $40 \mu\text{gm/cm}$  (i.e.,  $1.2 \times 10^{18}$  neon atoms per cm). This mass is  $\sim 30\%$  larger than required for maximum K-shell emission.<sup>9</sup>

X-ray spectra were collected for implosions using the PEOS with 1-MA peak current as shown in Fig. 1b. In this case the current risetime is 20 to 30 ns, and the implosion occurs 104 ns after onset of the current. This implosion corresponds to a mass loading of  $25 \mu\text{gm/cm}$  (i.e.,  $0.75 \times 10^{18}$  neon atoms per cm).

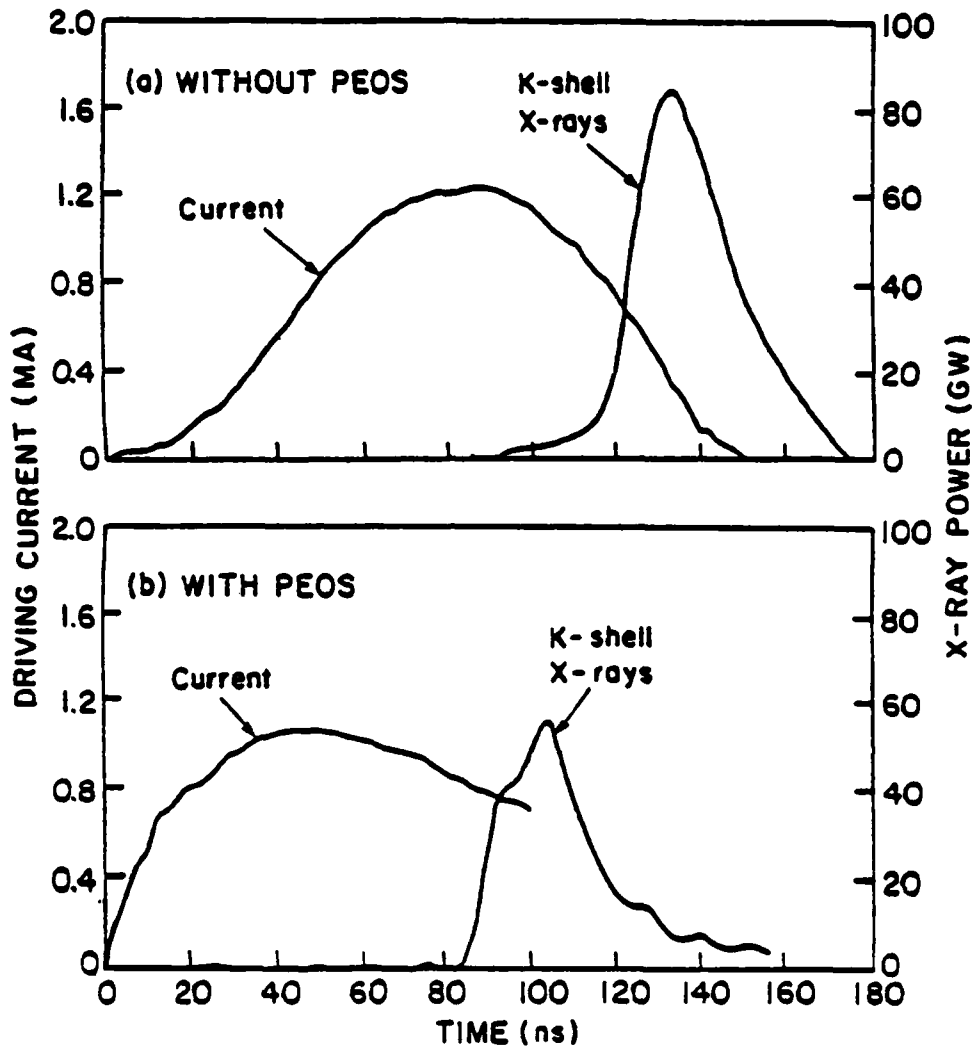


Fig. 1 — Current and x-ray traces for shots (a) without the PEOS and (b) with the PEOS

## B. Spectrograph

A potassium acid phthalate (KAP) convex crystal spectrograph provided good resolution in the spectral range of interest (900-1600 eV).<sup>15</sup> Kodak direct exposure film (DEF) was selected for high sensitivity as well as low fog level in the 8-15 Å region of interest.<sup>16</sup> A thin beryllium window (10 or 14 μm thick) was used in front of the spectrograph to filter unwanted radiation and to serve as a debris shield for the KAP crystal. For most observations a 0.25 mm wide imaging slit, located in front of the filter, was oriented perpendicular to the plasma axis to provide spatial resolution along the plasma column as sketched in Fig. 2. The spectrograph-to-source distance varied from 50 to 150 cm depending on the anticipated intensity, and the width of the imaging slit was varied accordingly.

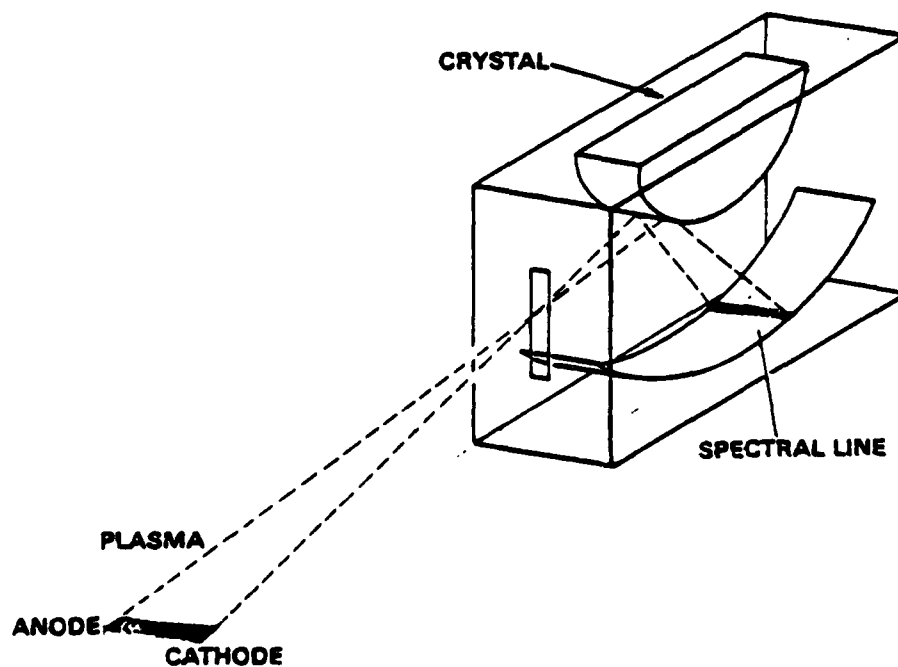


Fig. 2 — Experimental arrangement for spatial resolution of plasma source with x-ray crystal spectrograph

### III. DATA ANALYSIS

#### A. Processing of spectral films

Film densities were recorded across the spectra, i.e., along the dispersion direction, using a computerized scanning microdensitometer with a 10  $\mu\text{m}$  wide, 1 mm long slit. Exposures obtained on DEF film from monochromatic x-ray sources of known intensity in the same wavelength range were densitometered under the same conditions to provide absolute film calibrations. The film densities were converted to x-ray intensities in photons/cm<sup>2</sup> using a computer program which processes the data to derive the source intensity (in photons/sr. Å). Input were the integrated diffraction coefficients for the curved crystal,<sup>17</sup> published data on beryllium absorption coefficients, and the exposure - film density values derived from calibrated H-D curves obtained for the Kodak DEF emulsion.<sup>16</sup> A geometry factor F was used to account for the imaging slit effect in restricting the crystal illumination. Thus, the source intensity in terms of the energy radiated over a spectral interval  $d\lambda$ ,  $\int I(\lambda)d\lambda$ , is given by the summation computed by the program,  $\sum I(\lambda)\Delta\lambda$ , with:

$$\int I(\lambda)d\lambda = 4\pi F \cdot \sum I(\lambda)\Delta\lambda \quad (1)$$

The wavelength intervals  $\Delta\lambda$  were straightforwardly associated with the computerized microdensitometer recordings. Values of the source correction factor F, calculated for each set of geometrical parameters, are tabulated in the Appendix.

The energy radiated in a given discrete transition was obtained either directly from the computed intensity values summed over the line profile or

from a least-square fit of the computed intensity profile (Gaussian) taken above background. The latter derivation is required whenever the film background contribution is not negligible with respect to the line itself. The total radiation energy integrated over the spectral range recorded (-900-1600 eV) was also computed by the program. A correction for the background level on the emulsion was applied by measuring an average background density outside the spectral image on the film and converting it into the "equivalent" background intensity at each wavelength as computed by the program. The summation over our spectral range is then subtracted from the computed total energy. Similarly, the correct spectral intensity trace is obtained by subtracting, at each point, the background equivalent intensity from the computed one.

#### B. Atomic parameters for Neon

Neon K-shell discrete transitions consist of the  $np-1s$  series of Ne IX (helium-like) and Ne X (hydrogen-like) ions. The first lines of each ion main series are listed in Table I together with some basic atomic parameters. The line wavelengths for Ne X are taken from the computations of Garcia and Mack (18) while the energy levels of Ne IX are extracted from the tables of Ermolaev and Jones (19) which are based on refined calculations of two-electron ion states. The radiative probabilities,  $A$ , and oscillator strengths,  $f$ , were computed using the atomic structure code provided by Cowan.<sup>20</sup>

### IV. RESULTS

X-ray spectra obtained for a typical shot without the PEOS are shown in Fig. 3. These absolute intensity traces were obtained at three different

Table I — Ne IX and Ne X Transitions

Ne IX		1s <sup>2</sup> -1snp series		I.P. 1196 eV
n	λÅ	E <sub>ev</sub>	x 10 <sup>12</sup> $\frac{A}{sec^{-1}}$	f
2 He-α	13.447	922	9.16	0.75
	.55		0.0043	0.0004
3 He-β	11.547	1074	2.62	0.16
4 He-γ	11.000	1127	1.10	0.06
5 He-δ	10.76	1151	0.57	0.03
6	10.64	1164	0.337	0.017
7	10.56	1173	0.22	0.011

Ne X		1s-np series		I.P. 1362.16 eV
n	λÅ	E <sub>ev</sub>	x 10 <sup>12</sup> $\frac{A}{sec^{-1}}$	f
2 Lα	12.134	1022	12.55	0.416
3 Lβ	10.239	1211	3.35	0.079
4 Lγ	9.708	1277	1.36	0.029
5	9.481	1308	0.69	0.014
6	9.362	1324	0.39	0.0078
7	9.291	1334	0.25	0.0048

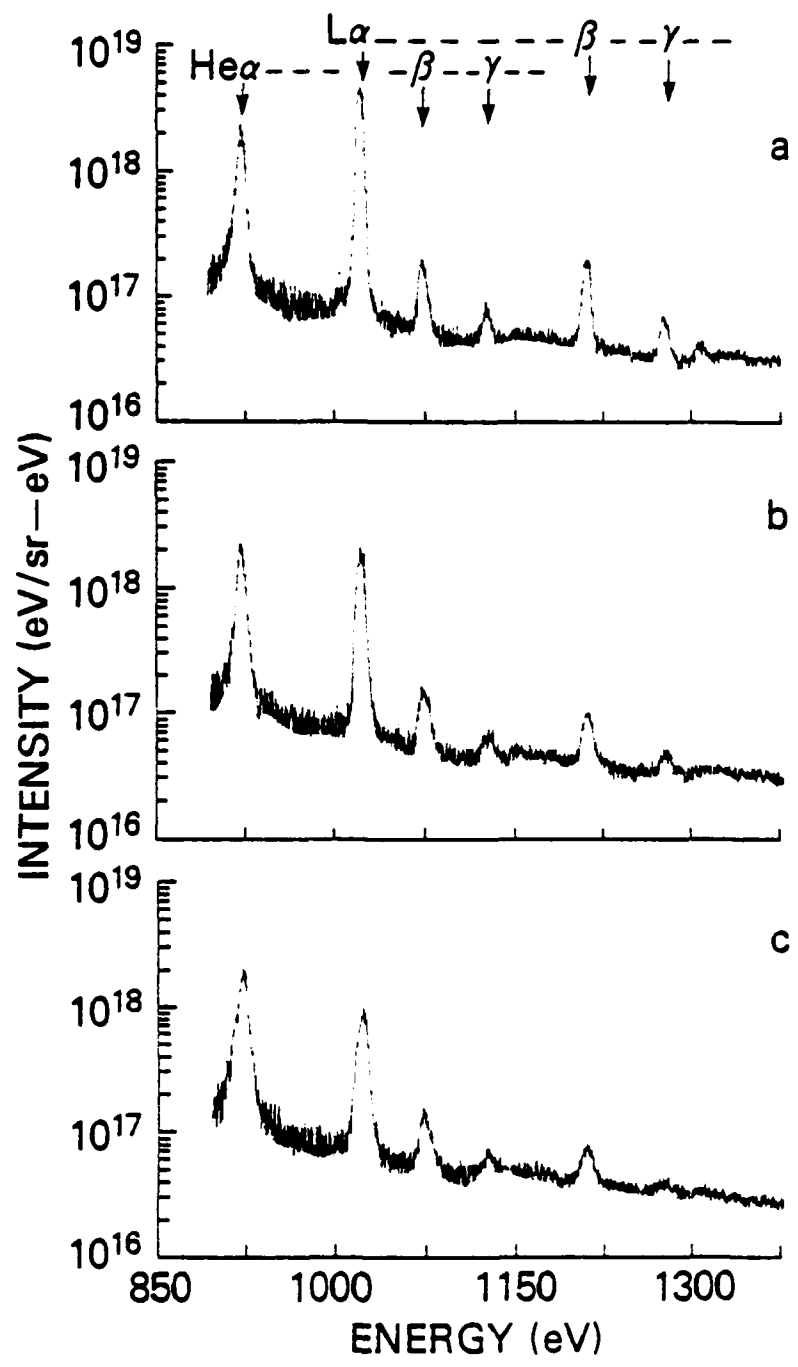


Fig. 3 — Intensity traces with Ne IX and Ne X lines from plasma generated without PEOS at three different locations: (a) plasma adjacent to cathode (b) 1.7 cm away from cathode (mid-gap) (c) 2.5 to 3 cm away from cathode (anode vicinity)

locations across the anode-cathode gap, namely near the cathode, at mid-electrode gap and near the anode. For He-like and H-like ions, the  $\alpha$ ,  $\beta$ , and  $\gamma$  lines are measurable above the free-free continuum and are identified. Similar spectral traces are shown in Fig. 4 for a shot with the PEOS at the same three locations along the Z-pinch. Implosions with the PEOS, have less background radiation and narrower lines so that, the higher Rydberg lines and the free-bound continuum are observed. Line peaks, up to transitions from the 6p level, are clearly identified above the background for both the Ne IX and X series. These intensity traces are on a log scale to emphasize weaker portions of the spectra. Intensity traces from the plasma region near the cathode are shown on a linear scale in Fig. 5. The linear intensity plots emphasize the fact that most of the x-ray emission occurs in the He $\alpha$  and L $\alpha$  lines at 922 and 1022 eV respectively. In Fig. 3,4, and 5 the ordinates are the converted spectral intensities not the absolute ones (factor  $4\pi F$  in Eq. (1) is omitted).

Spatially resolved images of the x-ray emission from these two neon implosions were obtained with time-integrated pinhole photography. X-rays were imaged through a pinhole onto Kodak no screen film located 74 cm from the implosion. A 6.4- $\mu$ m thick aluminum foil was placed in front of the film to filter low energy x-rays and a magnification of 0.75 was used. Pinholes of 0.05 and 0.13 mm diameter were used for the shot without a switch and for the shot with a PEOS, respectively. These x-ray images are displayed in Fig. 6, the image in Fig. 6b being overexposed. Note that return current rods (see Ref. 9) restrict full viewing of the plasma diameter while the diagnostic port obscures imaging the cathode vicinity, as indicated in Fig. 6. The spatial regions corresponding to the spectral measurements in Figs. 3 and 4 are

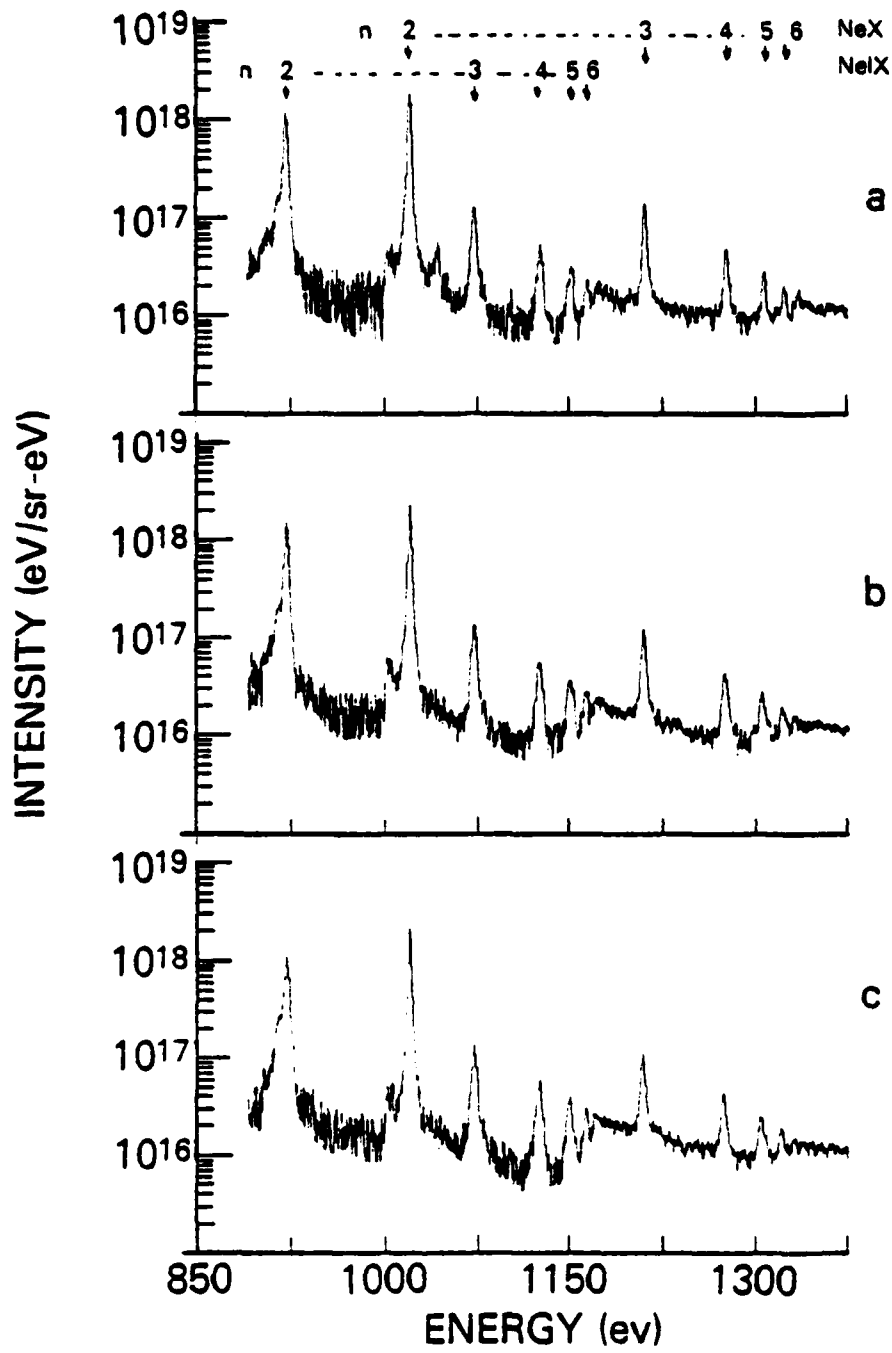


Fig. 4 — Intensity traces with Ne IX and Ne X lines from plasmas generated with PEOS at some locations (a) (b) (c) as in Fig. 3

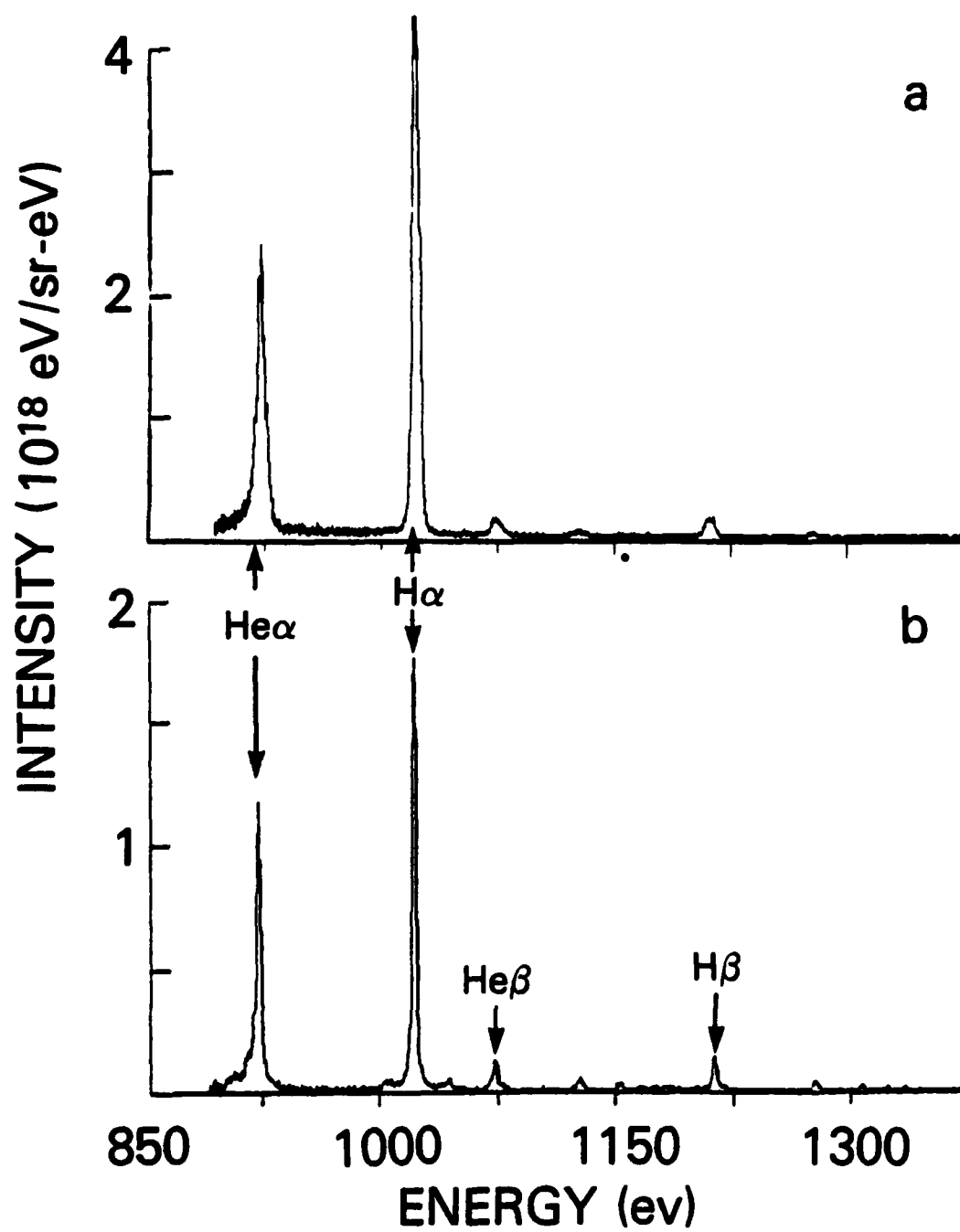
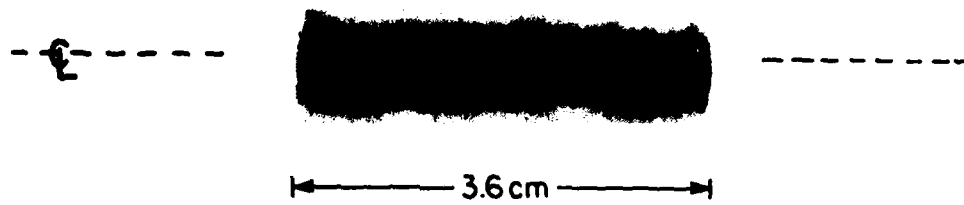
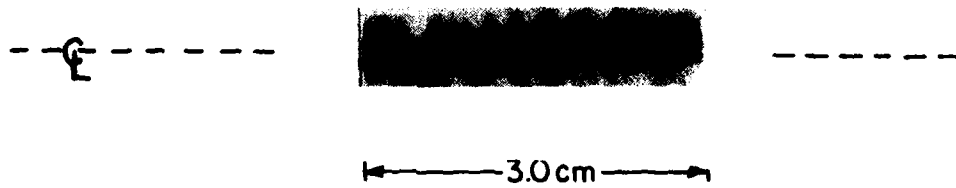


Fig. 5 - Comparison of neon spectral intensity for (a) the shot without the PEOS and (b) the shot with the PEOS. (Note the ordinate scale change of a factor of 2.)

a) WITHOUT PEOS



b) WITH PEOS



c) ANODE-CATHODE GEOMETRY

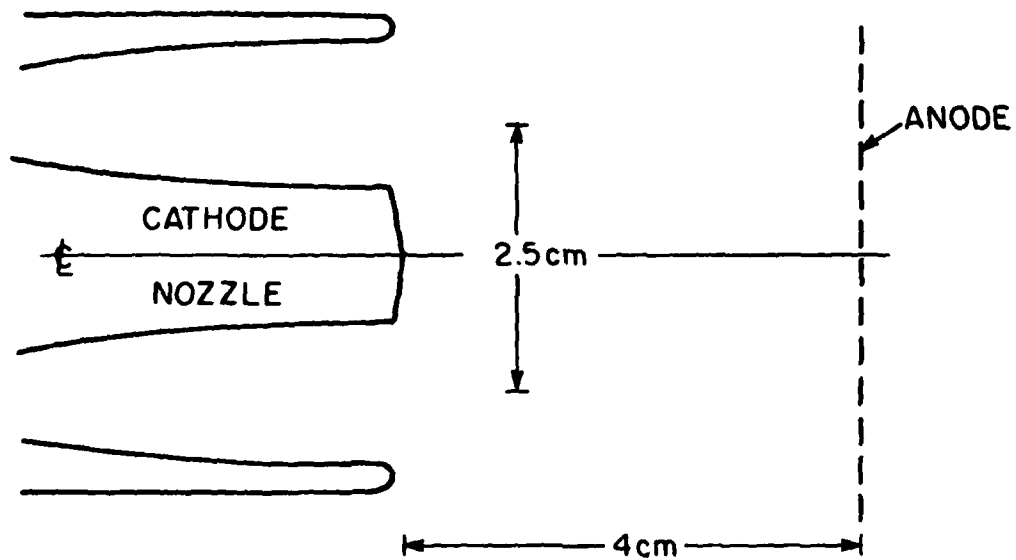


Fig. 6 — X-ray pinhole images of neon gas-jet implosions for (a) the shot without the PEOS and (b) the shot with the PEOS. The anode-cathode geometry corresponding to these images is shown in (c).

indicated in this figure. Comparison of these images indicates that the pinch with the PEOS is more confined radially and more uniform axially. The axial nonuniformity, or lack thereof, in these shots is quantified by the spectral intensity determinations reported below.

Absolute line intensities for these two shots are given in Table II for the first three lines in each series. The values quoted for three locations along the plasma represent the total energy radiated in each line based on the assumption that the emission from the whole plasma length is uniform. Since the measurements indicate that this is not the case (particularly for the shot without a switch), the correct total energy emitted from the source in each line is the mean of the tabulated values. The length of plasma column which produces measurable film density is derived from the line length observed on the film (perpendicular to the dispersion direction). Details are given in the Appendix. The observed plasma length is found to be 3.4 and 3.2 cm respectively for these two shots, in agreement (within 10%) with the pinhole images of the same shots (see Fig. 6). We also list in Table II the sum of the line energies from all discrete transitions and the total energy from lines and continuum, radiated over the observed spectral range (-900 - 1600 eV).

A most striking observation from Table II is that about 90% of the line radiation from the neon plasma is contained in the two  $\alpha$  lines. One notes a more uniform spectral line intensity as a function of interelectrode distance with the PEOS than without. However, for both discharge types, the  $\beta/\alpha$  line intensity ratios remain reasonably constant with values of ~10% for the He-like lines and ~5% for the H-like lines. Also, we find that ~75% of the total x-ray emission is contained in the lines for the PEOS shot, while the lines

Table II — Neon Line Absolute Intensities (Joules)

Plasma region	He <sup>II</sup>	He <sup>II</sup> β	He <sup>II</sup> γ	L <sup>α</sup>	L <sup>β</sup>	L <sup>γ</sup>	Total Spectral emission lines only	Total Spectral emission all spectrum	He <sup>II</sup> +L <sup>α</sup> Total line	He <sup>II</sup> +L <sup>α</sup> Total
AA	13.46	11.54	11	12.13	10.24	9.71				
C B A	500	40	10	890	41	10	1500	3000	0.93	0.46
	530	50	9.5	470	24	-5	1100	2400	0.91	0.42
	460	30	-9	230	16	4.6	750	2200	0.92	0.31
C B A	290	26	7	440	22	7	800	1100	0.91	0.66
	360	31	11	490	22	7	930	1200	0.91	0.71
	350	35	15	560	23	9	1000	1350	0.91	0.67

C cathode region (adjacent)  
 B mid-gap (1.7 cm from cathode)  
 A near anode (~3 cm from cathode)

contain only ~45% of the total for the shot without the switch (see Table II).

There are significant shot-to-shot variations in the intensity of the x-ray emission in this experiment. Without the PEOS, the total radiated energy (lines and continuum) from the spectrometer measurements varies between 1.6 and 2.5 kJ with the variation due primarily to changes in the background. A larger variation of 1.25 to 3 kJ is observed for the XRD on the same shots. This increased variation may be attributed to the energy dependent sensitivity of the XRD which produces different responses as the x-ray spectrum changes from shot-to-shot. For shots with the PEOS, the total x-ray output ranges from 0.9 to 1.2 kJ for the spectrometer; while the XRD gives ~1.5 kJ. These shot-to-shot variations are less for shots with the PEOS because the background contributes less to these shots.

Time-resolved measurements of the total neon K-shell radiation were obtained with an aluminum-cathode XRD filtered with 13- $\mu$ m thick aluminum foil. The measured K-shell x-ray traces, shown in Fig. 1, represent emission in the energy region corresponding to the spectrographic results in Table II. The filter transmission<sup>21</sup> and cathode response<sup>22</sup> for this XRD indicate that the detector sensitivity increases by more than a factor of twenty from 900 eV to 1560 eV (aluminum K-edge). Since most of the radiation from these neon implosions is emitted in the He- $\alpha$  and L- $\alpha$  lines, a detector sensitivity of 0.2 A/MW at 1000 eV was used to deduce the x-ray powers given in Fig. 1. These x-ray signals were integrated to estimate total radiated energy outputs. The measurements give 3.1 kJ for the shot without a switch and 1.5 kJ for the shot with a PEOS. These results are ~20% higher than total intensities from Table II (i.e., 2.5 kJ without the PEOS and 1.2 kJ with the PEOS). This difference is attributed to uncertainty in the XRD sensitivity. For example, evaluating

the XRD sensitivity at 1020 eV, rather than 1000 eV, results in a 20% increase in detector sensitivity and a 20% decrease in total energy output.

For the most intense Ne IX and Ne X lines we measured line widths from the reduced line profiles for a shot without and a shot with a PEOS. Table III lists full widths at half maximum measured at three positions along each spectral line corresponding to three locations (C,B,A) along the plasma axis (indicated in Table III). The lines are narrower by a factor of about 2 for the shot with the PEOS.

Table III — Observed F.W.H.M.,  $\Delta\lambda$ , of some Ne IX and Ne X lines in Å

plasma region		He $\alpha$	He $\beta$	La	L $\beta$
without PEOS	C	0.08	0.08	0.068	0.06
	B	0.10	-0.10	0.08	0.08
	A	0.10	0.09	-0.1	0.08
with PEOS	C	0.045	0.044	0.034	0.027
	B	0.047	-	0.033	-
	A	0.056	0.040	0.026	0.028

C cathode region (adjacent)

B mid-gap (1.7 cm from cathode)

A near anode (-3 cm from cathode)

## V. Summary

X-ray spectroscopy with established x-ray film calibrations and crystal responses has provided absolute intensities for neon K-shell x-rays from gas-jet implosions. Most (90%) of the line radiation is contained in the He- $\alpha$  and L- $\alpha$  lines of neon. The use of a PEOS to reduce the current risetime and eliminate prepulse produces spectra with less continuum background and with lines that are narrower by a factor of two. With the PEOS and 1-MA peak driving current, the total radiated energy from 900 to 1600 eV is 1.2 kJ with ~75% of this emission in line radiation. Without the PEOS and with 1.2 MA peak driving current, the total radiated energy in this energy region increases to 2.5 kJ, but only ~45% is in line radiation.

Although time-resolved data are needed for any discussion of basic processes in plasma formation, these space-resolved but time-integrated results suggest that temperature/density variations exist along the plasma length, as well as non-uniform ionic populations. These quantitative spectroscopic measurements demonstrate that the imploded plasmas generated with the PEOS are more uniform, in agreement with pinhole photography.

Appendix

Geometrical Source Factor

The spectral line length on the film is determined by: (Fig. A1)

- (1) the distance L between light source and crystal
- (2) the front slit width d

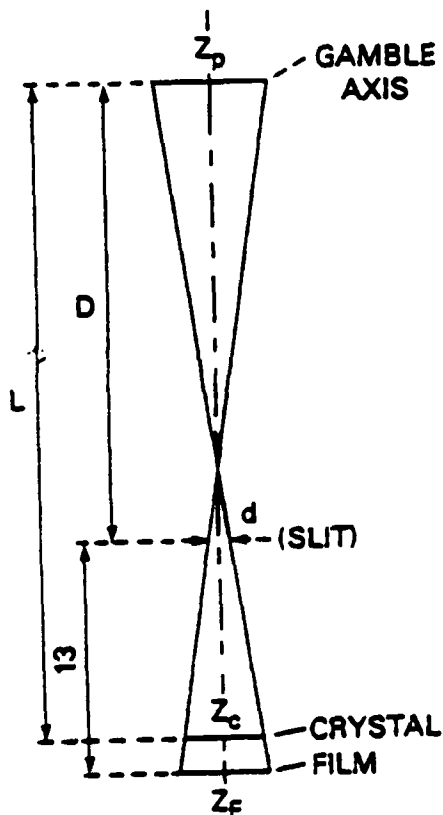


Figure A1

The following relation between

Z<sub>p</sub>: (plasma length on axis)

and Z<sub>F</sub>: (illuminated length on film for a spectral line) is derived straightforwardly:

$$Z_F = d + 13 \cdot \frac{d + Z_p}{D} \quad (A1)$$

with cm units where D is the distance between light source and slit. The average distance between the slit and the film in the spectrograph is 13 cm.

Similarly each point on the film is illuminated by a length of plasma d<sub>p</sub> with:

$$d_p = d \cdot \frac{D + 13}{13} \quad (A2)$$

rather than by the whole plasma length, Z<sub>p</sub> = 4 cm.

The geometrical factor  $F$  associated with this spectral imaging that restricts the film illumination is defined as:

$$F = \frac{Z_p}{d_p} = \frac{D(Z_F - d) - 13d}{d(D + 13)} \quad (A3)$$

and is derived for each set of observation conditions.

Practically, the useful length of plasma producing a measurable intensity on the film is derived from  $Z_F$ , the measured line length along the film perpendicular to the dispersion ( $\lambda$ ) direction, as indicated in Eq. A1.

The values used for the geometrical factors  $F$  are listed in Table A together with the corresponding geometrical parameters. Consistent intensity values were obtained for the various geometrical conditions (different  $F$  factors), and the total radiated energy values derived from the spectra (Table II) agree within 25% with XRD measurements of the K-shell yield. The results in Table II are based on shots #2849 (no PEOS) and #2594 (with PEOS). We note that the standard (0.25 mm wide) slit provides a spatial resolution of about 2 mm along the plasma. Spectra taken at maximum distance ( $D = 150$  cm, no slit) yielded directly the intensities from the whole plasma, without any geometrical source factor ( $F = 1$ ). Practically, the best intensity ratios for the  $\beta$  and  $\gamma$  lines (He-like and H-like) were obtained with these conditions (shot #2870). These more intense spectra (without slit) also allowed accurate measurements of the recombination continuum onset (#2868 and #2870).

Table A — Geometrical Parameters (in cm) and F Factors

Shot #	Observed $Z_F$	D	d	F
2531	0.63	79	0.025	20.6
2585*	0.54	79	"	17.5
2594*	0.56	79	"	18.2
2668	0.41	109.5	"	13.7
2846	0.8	50	"	24.4
2849	0.58	79	"	18.9
2865	0.44	109.5	0.06	5.5
2868	0.75	109.5	0.6	1
2870	0.55	150	0.6	1

\*shots generated with a PEOS

### References

- (1) J. Shiloh, A. Fisher and N. Rostoker, Phys. Rev. Lett. 40, 515 (1978).
- (2) P.G. Burkhalter, J. Shiloh, A. Fisher and R.D. Cowan, J. Appl. Phys. 50, 4532 (1979).
- (3) C. Stallings, K. Childers, I. Roth and R. Schneider, Appl. Phys. Lett. 35, 524 (1979).
- (4) W. Clark, R. Richardson, J. Brannon, M. Wilkinson and J. Katzenstein, J. Appl. Phys. 53, 5552 (1982).
- (5) C.D. Challis, A.E. Dangor, E.S. Wyndham, D. Mosher, W.G. Bessell and D.J. Bond, in Proc. 11th European Conf. Controlled Fusion and Plasma Physics, Aachen, (1983).
- (6) R.B. Spielman, D.L. Hanson, M.A. Palmer, M.K. Matzen, T.W. Hussey and J.M. Peek, J. Appl. Phys. 57, 830 (1985).
- (7) S.J. Stephanakis, J.R. Boller, G. Cooperstein, R.A. Meger, J.M. Neri, P.F. Ottinger, F.C. Young, D.J. Nagel, J. Davis, D.P. Duston and P.C. Kepple, Record.-Abstr. 1984 IEEE Inter. Conf. Plasma Sci., St. Louis, 1984, p 9.
- (8) P.F. Ottinger, S.A. Goldstein and R.A. Meger, J. Appl. Phys. 56, 774 (1984).
- (9) S.J. Stephanakis, J.P. Apruzese, P.G. Burkhalter, J. Davis, R.A. Meger, S.W. McDonald, G. Mehlman, P.F. Ottinger and F.C. Young, Appl. Phys. Lett., 48, 829 (1986).
- (10) J.P. Apruzese, J. Davis and K.G. Whitney, J. Appl. Phys. 53, 4020 (1982).
- (11) R.C. Elton, T.N. Lee and P.G. Burkhalter, Nucl. Instr. Meth. Phys. Res. 39, 753 (1985).

- (12) XTLFILM program, unpublished, R.R. Whitlock, J.W. Criss, B. Sweeney and D.A. Newman, Code 4680 NRL.
- (13) R.S. Smith, W.O. Doggett, I. Roth and C. Stallings, Appl. Phys. Lett. 41, 572 (1982).
- (14) S.W. McDonald and P.F. Ottinger, Naval Research Laboratory, Memo Report #5785.
- (15) P.G. Burkhalter, D.B. Brown and M. Gersten, J. Appl. Phys. 52, 437 (1981).
- (16) P.D. Rockett, C.R. Bird, C.J. Hailey, D. Sullivan, D.B. Brown and P.G. Burkhalter, Appl. Optics 24, 2536 (1985).
- (17) D.B. Brown and M. Fatemi, J. Appl. Phys. 51, 2540 (1980).
- (18) J.D. Garcia and J.E. Mack, J. Opt. Soc. Am. 55, 654 (1965).
- (19) A.M. Ermolaev and M. Jones, J. Phys. B7, 199 (1974).
- (20) R.D. Cowan, J. Opt. Soc. Am. 58, 808 (1968).
- (21) Wm.J. Veigele, et al., Kaman Sciences Corporation Report DNA 2433 F, 1971 (unpublished).
- (22) J.R. Kerns and D.J. Johnson, J. Appl. Phys. 45, 5225 (1974).

END

10-86

DT/C